ORNL/TM-2021/2023

Development of an Activation Analysis Methodology to Support the Disposal of the High Flux Isotope Reactor Original Reflector Container

Jorge Navarro
Scott A. Byers
Randal E. Pudelek
Geoffrey G. Deichert
Young Soo Kwon
Russ Wools
Mathew A. Grooms

August 2021

OAK RIDGE National Laboratory

ORNL IS MANAGED BY UT-BATTELLE LLC FOR THE US DEPARTMENT OF ENERGY

ORNL/TM-2021/2023

Nuclear Energy and Fuel Cycle Division

DEVELOPMENT OF AN ACTIVATION ANALYSIS TO SUPPORT THE DISPOSAL OF THE HIGH FLUX ISOTOPE REACTOR ORIGINAL REFLECTOR CONTAINER

Jorge Navarro
Young Soo Kwon
Scott A. Byers
Randal E. Pudelek
Geoffrey G. Deichert
Russ Wools
Mathew A. Grooms
David G. Blanchard

Date Published: August,12, 2021

Prepared by
OAK RIDGE NATIONAL LABORATORY
Oak Ridge, TN 37831-6283
managed by
UT-BATTELLE, LLC
for the
US DEPARTMENT OF ENERGY

CONTENTS

LIST OF FIGURES

LIST OF TABLES

SUMMARY

The original beryllium reflector container was installed prior to the first High Flux Isotope Reactor (HFIR) cycle and was removed at the end of cycle 382. The original beryllium reflector was part of every HFIR irradiation cycle from September of 1966 to October of 2000. After its service lifetime, the beryllium reflector container was placed in interim storage at the spent fuel pool adjacent to the reactor. Due to space limitations in the spent pool fuel, the beryllium reflector container must be removed and sent to a location for permanent storage. Before the beryllium reflector container can be shipped, its radiological activity must be known. To determine the overall activity, the isotopic inventory, and the volumetric material fractions, as well as some of the original reflector container's stainless-steel quantities must be established. Therefore, a methodology was developed to determine a conservative activation scenario.

1. INTRODUCTION

The beryllium internal core change-out for High Isotope Flux reactor (HFIR) is scheduled during 2023. As part of the preparations needed to ensure a successful core internal change-out, legacy materials must be removed from the spent fuel pool and relocated to a long-term waste storage facility. The main purposes of removing the legacy material are (1) to ensure that operations personnel have enough space to maneuver during the core change-out, and (2) to store more material to be removed from the reactor. One legacy part that is being removed is the container that surrounded the permanent beryllium reflector. This container was in service as part of HFIR from the first reactor startup in September of 1966 to the end of cycle 382 in October of 2000. Before the beryllium reflector container is removed and transported from the fuel storage pool to a permanent waste site, the activation rate and isotopic inventory must be determined for transportation purposes.

2. PROBLEM STATEMENT

The difficulty of finding reliable and accurate history of the parts of interest poses a challenge to the process for determining the activation rate and the isotopic inventory of legacy reactor parts. In this particular case, the main challenge is to determine the fraction of stainless steel embedded in the container with relative accuracy. This is difficult to discern since the beryllium reflector container was manufactured over 50 years ago, and some highly activated stainless-steel pieces have been removed. To overcome this challenge, the strategy focused on performing two types of experimental dose rate measurements and two sets of computational analysis. The results of these measurements and analyses were then compared. The dose measurement data served as the initial conditions and as a tool to confirm isotopic data. The computational analyses were used to compute total activity, to determine a complete isotopic breakdown, and to determine the volumetric ration of aluminum to stainless steel. The first set of computational analysis used the reflector dose, which was measured experimentally as an initial condition, to compute total activity. The second computational analysis replicated the irradiation history of the reflector container, so a conservative estimate of the overall curie content and isotopic distribution could be determined. The two computational analyses were independent from each other, but the two methodologies were expected to show signs of convergence if the stainless-steel volumetric fraction were similar.

3. DOSE RATE AND ISOTOPIC DISTRIBUTION METHODOLOGY DEVELOPMENT

3.1 EXPERIMENTAL MEASUMENTS

The first set of experimental measurements were in-air surveys (HFIR-537801 - Survey for flashing beryllium cage). The survey map shows the dose measurements recorded at close range (~4–10 inches). The higher exposure rates reported on the survey map were located around the middle of the reflector container, as shown on the southeast and Engineering Facility (EF) 1 regions of the survey map, respectively. Based on first round of exposure rate measurements, it was decided that a second round of exposure rate surveys (HFIR-554459: Cage 2-meter dose rates) should be conducted. The second round consisted of six measurements that were taken at 2 meters from the axial plane of the top and bottom ring at the beam tube's horizontal plane.

A second type of experimental measurements was performed in which a gamma camera was used to better understand the exposure rate distribution and to determine major gamma-emitting isotopes. In essence, the measurements were performed to ensure that only isotopic products derived from the activation of stainless steel and aluminum were present in the reflector container.

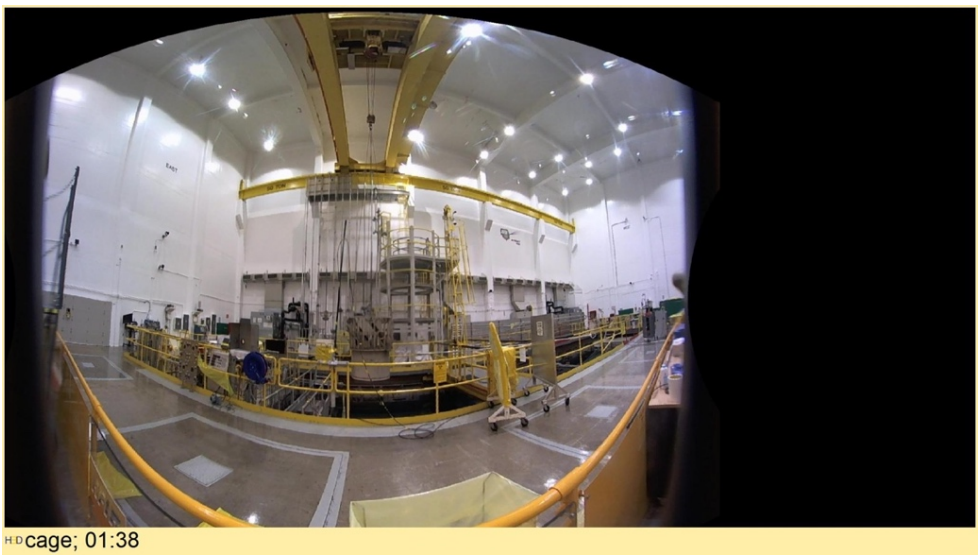

Figure 1. Gamma camera view of the reflector container.

Figure 1 shows the gamma camera's view of the reflector container as it was taken out of the spent fuel pool for measurements. Figure 2 shows the gamma spectrum signal that was emitting from the reflector container, and Figure 3 presents the dose map obtained by the gamma camera. As shown in Figure 2, the peaks in the spectrum correspond to ^{60}Co.

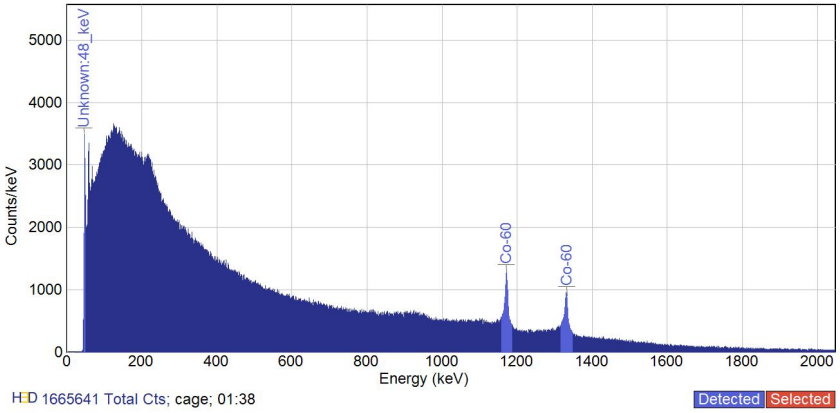

Figure 2. Cage gamma spectrum.

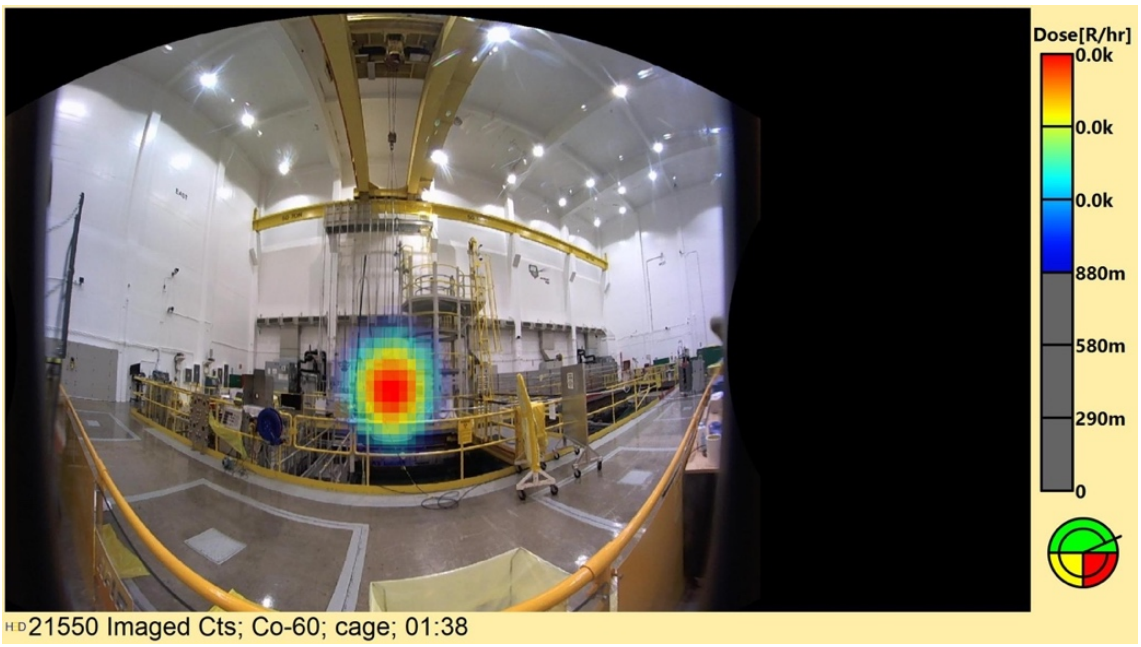

Figure 3. Dose location image.

4. MICROSHIELD ANALYSIS

4.1 MICROSHIELD ANALYSIS DESCRIPTION

A model of the beryllium reflector cage was developed and analyzed using MicroShield Version 8.03 (Grove Software, 2006). Additional in-air surveys of the cage were conducted on March 11, 2021: this survey (HFIR-554459: Cage 2-meter dose rates) consisted of 6 measurements taken at 2 meters from the axial plane of the top and bottom ring at the beam tube's horizontal plane. These locations were chosen because previous surveys showed this to be the area with the highest activity. The 2-meter distance was chosen because it is a sufficient distance to determine the effect from the cage's overall activity. These measurements can then be used to empirically estimate the cage activity.

4.2 METHODOLOGY

The model was used to estimate the expected exposure rate from 1 Ci of ^{60}Co. Based on this modeled exposure rate and the measured exposure rate from the 2-meter surveys, the amount of the cage's ^{60}Co activity can then be estimated, and then the other radionuclides are scaled based on the isotopic distributions presented from Section 5.1. This dose-to-curie methodology allows the overall activity for each radionuclide to be determined.

4.3 MICROSHIELD MODEL

4.3.1 GEOMETRY

The cage was modeled in MicroShield as an annual cylinder with an inner radius of 21.375 inches (54.2925 cm), a source thickness of 4.75 inches (12.065 cm), and a height of 31.75 inches (80.645 cm). These dimensions were based on HFIR drawings of the cage, in which the thickness was determined based on the average of the maximum horizontal dimension of the ribs. This results in a modeled source volume of

3.6879E+05 cm^3. The height was conservatively based on the cage and pedestal assembly, resulting in lower modeled dose rates for an activity of 1 Ci ^{60}Co.

4.3.2 MATERIAL AND EFFECTIVE DENSITY

The material is primarily aluminum, with an effective density of 1.15 g/cm^3. This was determined first by calculating the mass of the cage using the volume of 9,587.73 ft^3 (1.57E+05 cm^3), as provided in Table 9, and multiplying by 2.7 g/cm^3, the density of aluminum, resulting in a mass of 4.24E+05 g. This mass was divided by the volume of the annular cylinder model with the dimensions of 3.6879E+05 cm^3 from the modeled source volume. This effective density is a necessary approximation due to the simplified MicroShield models and ensures the model's self-shielding characteristics are representative of the cage's self-shielding characteristics.

4.3.3 SOURCE TERM

The source used for the model was assumed to be 1 Ci (3.7E10 Bq) of ^{60}Co. This was based on the isotopic distribution from Table 5 and Table 6, as well as the actual measurement from the gamma camera. This distribution shows many of the radionuclides other than ^{60}Co (>99%) are beta emitters or low-energy gamma emitters, which are difficult to detect with the ion chamber used for the 2-meter survey. Therefore, the measured exposure rate from the cage was conservatively assumed to be solely from ^{60}Co photons. Using 1 Ci as the activity allows for scaling the activity with the empirical measurements to estimate the ^{60}Co activity, and therefore the total radionuclide inventory.

4.3.4 DOSE POINT LOCATIONS

During the survey of the cage, the distance from the detector to the cage was measured and ensured to be at 2 meters. The dose point for the MicroShield model was calculated to coincide with the 2-meter dose measurements. Based on the HFIR drawings, the upper ring outer radius is 23.75 inches (60.325 cm). The dose point was assumed to be 260.325 cm from the centerline of the annular cylinder, or 2 meters from the outer circumference of the upper ring. The height of the dose point was assumed to be at the beam tube plane of the cage, which is 17.250 inches from the top, or 43.125 inches (109.5375 cm) from the bottom of the annular cylinder (conservative for activity calculation purposes). This dose point location results in a lower exposure rate per curie for the model, resulting in higher activity for a given measured exposure rate.

4.3.5 SURVEY DATA

The cage was surveyed on March 11, 2021, and measurements were taken at 5 locations. Exposure rates averaged 620 mR/h, with a maximum of 700 mR/h (see Figure 4). This survey was performed with a Ludlum 9-4 ion chamber survey instrument.

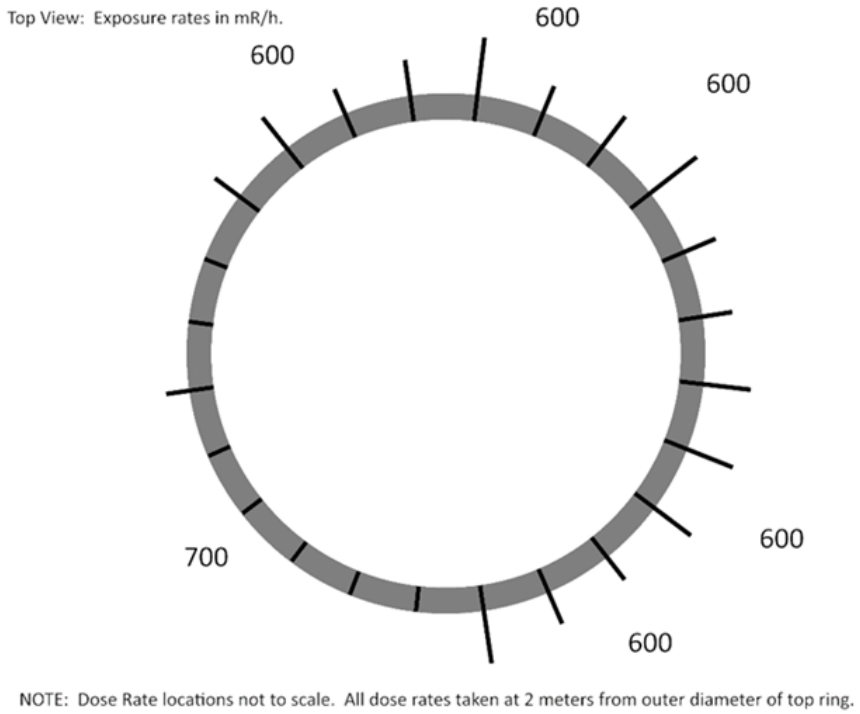

Figure 4. Cage exposure rates (mR/h) 2m axially from top ring at beam port elevation.

4.3.6 MICROSHIELD RESULTS

The MicroShield model resulted in a 2-meter exposure rate of 126.9 mR h^{-1} Ci^{-1} of ^{60}Co. Based on the average exposure rate of 620 mR/h, the cage's ^{60}Co activity was estimated to be 4.89 Ci (620 mR h^{-1} / 126.9 mR h^{-1} Ci^{-1}). APPENDIX B shows the MicroShield output.

Based on the material isotopic distributions provided in Table 7 and Table 8, the distribution for various mixtures of volumetric percentages of aluminum and stainless steel can be determined. From these isotopic distributions, the estimated activity can be determined by scaling the ^{60}Co to the other radionuclides. The distributions and resulting activities for various aluminum volumetric fractions are shown in Table 1 and Table 2. This activity is significantly less than the activity determined using the methodology described below in Section 5.1. This demonstrates that methodology is conservative and bounding.

Table 1. Radionuclide activity fraction at various aluminum volumetric fractions

	Radionuclide activity fraction									
Nuclide	**99.2% Al**	**99.3% Al**	**99.4% Al**	**99.5% Al**	**99.6% Al**	**99.7% Al**	**99.8% Al**	**99.9% Al**	**99.98% Al**	**100.0% Al**
^{3}H	1.06E-03	1.21E-03	1.40E-03	1.67E-03	2.07E-03	2.70E-03	3.90E-03	6.98E-03	1.90E-02	3.35E-02
^{26}Al	1.10E-06	1.25E-06	1.45E-06	1.73E-06	2.14E-06	2.79E-06	4.03E-06	7.23E-06	1.97E-05	3.47E-05
^{14}C	1.17E-08	1.17E-08	1.16E-08	1.15E-08	1.14E-08	1.12E-08	1.07E-08	9.60E-09	5.23E-09	0.00E+00
^{32}Si	2.81E-09	3.19E-09	3.71E-09	4.42E-09	5.46E-09	7.14E-09	1.03E-08	1.85E-08	5.04E-08	8.86E-08
^{32}P	2.81E-09	3.19E-09	3.71E-09	4.42E-09	5.46E-09	7.14E-09	1.03E-08	1.85E-08	5.04E-08	8.86E-08
^{55}Fe	5.29E-01	5.29E-01	5.29E-01	5.30E-01	5.30E-01	5.30E-01	5.31E-01	5.32E-01	5.37E-01	5.43E-01
^{60}Fe	1.98E-08	2.26E-08	2.62E-08	3.12E-08	3.86E-08	5.04E-08	7.28E-08	1.30E-07	3.56E-07	6.26E-07
^{60}Co	2.39E-02	2.57E-02	2.80E-02	3.13E-02	3.60E-02	4.37E-02	5.81E-02	9.53E-02	2.41E-01	4.15E-01
^{60m}Co	1.98E-08	2.26E-08	2.62E-08	3.12E-08	3.86E-08	5.04E-08	7.28E-08	1.30E-07	3.56E-07	6.26E-07
^{59}Ni	1.60E-03	1.59E-03	1.58E-03	1.57E-03	1.55E-03	1.52E-03	1.46E-03	1.31E-03	7.12E-04	0.00E+00
^{63}Ni	4.44E-01	4.42E-01	4.39E-01	4.36E-01	4.31E-01	4.22E-01	4.06E-01	3.65E-01	2.03E-01	8.67E-03
^{65}Zn	2.48E-09	2.83E-09	3.28E-09	3.91E-09	4.83E-09	6.32E-09	9.12E-09	1.64E-08	4.46E-08	7.84E-08

Table 2. Radionuclide Activities with 4.89 Ci-Co-60 (Curies)

Calculated Radionuclide Activities with 4.89 Ci Co-60 (Curies)										
Nuclide	**99.2% Al**	**99.3% Al**	**99.4% Al**	**99.5% Al**	**99.6% Al**	**99.7% Al**	**99.8% Al**	**99.9% Al**	**99.98% Al**	**100.0% Al**
^{3}H	2.17E-01	2.30E-01	2.45E-01	2.62E-01	2.81E-01	3.03E-01	3.28E-01	3.58E-01	3.87E-01	3.95E-01
^{26}Al	2.25E-04	2.38E-04	2.53E-04	2.71E-04	2.90E-04	3.13E-04	3.40E-04	3.71E-04	4.01E-04	4.09E-04
^{14}C	2.40E-06	2.23E-06	2.03E-06	1.80E-06	1.55E-06	1.25E-06	9.03E-07	4.93E-07	1.06E-07	0.00E+00
^{32}Si	5.74E-07	6.08E-07	6.47E-07	6.91E-07	7.41E-07	8.00E-07	8.68E-07	9.48E-07	1.02E-06	1.04E-06
^{32}P	5.74E-07	6.08E-07	6.47E-07	6.91E-07	7.41E-07	8.00E-07	8.68E-07	9.48E-07	1.02E-06	1.04E-06
^{55}Fe	1.08E+02	1.01E+02	9.24E+01	8.29E+01	7.20E+01	5.94E+01	4.47E+01	2.73E+01	1.09E+01	6.40E+00
^{60}Fe	4.05E-06	4.30E-06	4.57E-06	4.88E-06	5.24E-06	5.65E-06	6.13E-06	6.70E-06	7.23E-06	7.38E-06
^{60}Co	4.89E+00	4.89E+00	4.89E+00	4.89E+00	4.89E+00	4.89E+00	4.89E+00	4.89E+00	4.89E+00	4.89E+00
^{60m}Co	4.05E-06	4.30E-06	4.57E-06	4.88E-06	5.24E-06	5.65E-06	6.13E-06	6.70E-06	7.23E-06	7.38E-06
^{59}Ni	3.27E-01	3.03E-01	2.76E-01	2.45E-01	2.10E-01	1.70E-01	1.23E-01	6.70E-02	1.45E-02	0.00E+00
^{63}Ni	9.08E+01	8.42E+01	7.67E+01	6.82E+01	5.85E+01	4.73E+01	3.42E+01	1.87E+01	4.12E+00	1.02E-01
^{65}Zn	5.08E-07	5.38E-07	5.73E-07	6.12E-07	6.56E-07	7.08E-07	7.68E-07	8.39E-07	9.06E-07	9.25E-07
Total	2.04E+02	1.90E+02	1.74E+02	1.56E+02	1.36E+02	1.12E+02	8.42E+01	5.13E+01	2.03E+01	1.18E+01

5. MCNP-ORIGEN ACTIVATION ANAYLSIS

5.1 COMPUTATIONAL ANALYSIS TO DETERMINE A CONSERVATIVE DOSE RATE AND ISOTOPIC DISTRIBUTION

As stated above, the original beryllium reflector container is mostly made of aluminum with some stainless-steel pieces in the form of helicoils, bolts, pins, O-rings, washers, hex screws and nuts. An operation was performed to remove the stainless steel. The process consisted of removing as much stainless steel as feasible given the need for underwater disassembly and sawing operations. In addition, the removal operation was also limited by concerns to maintain exposure as low as reasonably achievable (ALARA). Based on the removal operation, the leftover stainless material was conservatively estimated to be less than 0.1% of the overall container by the spent pool operators. Therefore, the main challenge became determining the overall isotopic content. To determine the overall isotopic breakdown and a bounding activation scenario, and also to confirm experimental-based exposure rate estimations, a conservative methodology was developed.

5.1.1 CONSERVATIVE METHODOLOGY DEVELOPMENT

The initial stage of the analysis consisted of modifying an existent Monte Carlo N-Particle (MCNP) (X-5 Monte Carlo Team, 2005) end of cycle (EOC) input model (G. Ilas, 2015). The main modification of the original input deck consisted of creating different axial and horizontal regions for original cage cell representation. The base model from G. Ilas, 2015, represented the beryllium container as three distinctive regions: a main body (continuous annular cylinder) and two additional regions representing the EF locations. The updated simulated cage was divided into 32 axial and horizontal zones of the main body, as well as two additional zones representing the EFs. The additional regions were created to better capture the flux variations across the cage component. Once those regions were added to the simulated reflector container, two analysis cases were developed and computed, as detailed below:

1. Aluminum case – material used for the 34 regions was Aluminum 6061 (Table 3)
2. Stainless steel case – material used for all 34 regions was Stainless Steel 304S (Table 4)

3. Table 3. Aluminum material mass composition

Aluminum 6061	High impurities content (mass %)
Silicon	0.8
Iron	0.7
Copper	0.4
Manganese	0.15
Magnesium	1.20
Chromium	0.35
Zinc	0.25
Titanium	0.15
Aluminum	96.00
Total	100.00

Table 4. Stainless Steel Mass Composition.

Stainless Steel 304	High impurities content (mass %)
Carbon	0.08
Silicon	1.00
Phosphorus	0.045
Chromium	19.00
Manganese	2.00
Iron	68.38
Nickel	9.50
Total	100.0

The two cases were developed because the principal unknown of this analysis is the amount of leftover stainless steel that remains embedded or attached to the beryllium reflector container. The strategy consisted of performing simulations for both cases to find the highest flux region value.

After the highest flux region value was determined, the total flux was used, along with the 44-group energy discretized flux for that region, as inputs for the activation calculation. Figure 5 shows a flowchart of the process, in which the 44-group energy discretized flux was used to calculate a one-group cross section using COUPLE (Hermann, 1984). A code that calculates a one-group collapsed problem's specific cross section as required for the ORIGEN-S (Hermann, O.W., 1984) activation calculation. Once the one-group's collapsed cross section was calculated for each material, it was used along with the total flux to determine a conservative isotopic content, as well as a total curie content per volume in ORIGEN-S (Hermann, O.W., 1984).

5.1.2 ASSUMPTIONS AND ANALYSIS PARAMETERS

The reflector's container structure was inserted into HFIR at the beginning of cycle 1, and it was removed after the end of cycle 382. The time period in which the aluminum cage was irradiated was from January of 1966 to October of 2000. During that period, three long outages occurred related to three different beryllium reflector replacements. A fourth outage also occurred that lasted 3½ years related to assessment of the HFIR pressure vessel. The result of the 3½-year outage was a reduction of power from 100 MW to 85 MW. For the development of the conservative methodology described herein, a power of 100 MW was used for all irradiation periods.

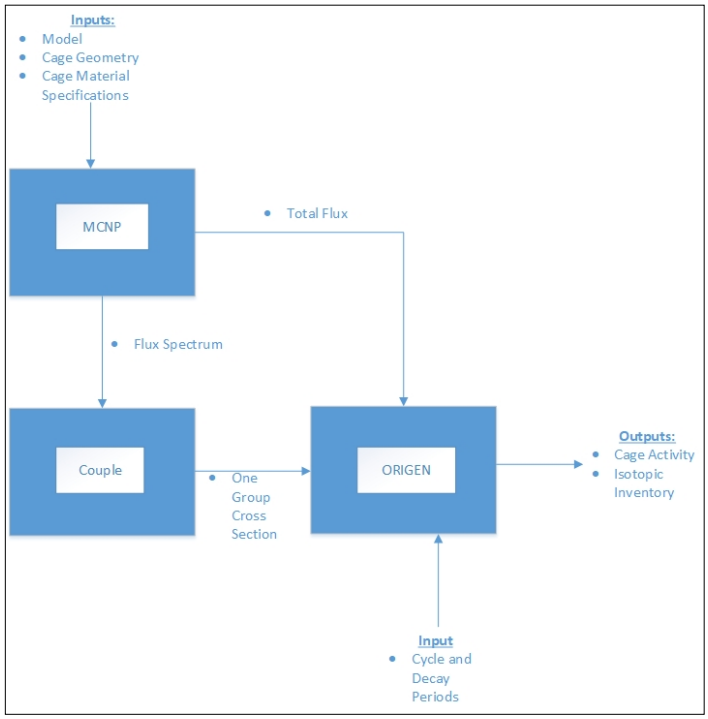

Figure 5 . Activity calculation flow chart.

The analysis methodology consisted of simulating eight time-steps: four irradiation periods, three outage intervals, and a cooldown phase. The methodology did not include downtime between cycles which will yield an overestimation of the total activation inventory, which is a conservative assumption. The analysis was performed assumed that the reactor operated 100% of the time except for the three outages shown in Table 5. The eight time-steps used for the activation calculations are summarized in Table 5 below.

Geometrical simplifications and assumptions were made during development and application of the methodology described in this report. The main geometrical assumption was to represent the cage as a continuous annular cylinder instead of modeling it as it was built. The representation of the reflector container is based on the original HFIR 400 cycle model unit cell. The second geometrical assumption was to model the reflector container with only two EFs, as it is represented in the most current reflector container, instead of with the four EFs initially contained in the original beryllium reflector container cage. These assumptions were used to simplify and expedite the analysis.

Table 5. Summary of irradiations and decay steps

Calculation Step	Step Type	Starting cycle	Final cycle	Starting Date	Final Date	Power (MW)	Total Days	Accumulated MWd
1	Irradiation	1	121	26-Jan-66	3-Jun-75	100	2,782.54*	278,254.00
2	Outage	-	-	3-Jun-75	29-Aug-75	-	87.00	-
3	Irradiation	122	244	29-Aug-75	20-Sep-83	100	2,703.40*	270,340.00
4	Outage	-	-	20-Sep-83	20-Dec-83	-	90.71	-
5	Irradiation	245	287	20-Dec-83	14-Nov-86	100	913.42*	91,342.00
6	Outage	-	-	14-Nov-86	18-May-90	-	1,280.83	-
7	Irradiation	288	382	18-May-90	1-Oct-00	100	1,886.45*	188,645.00
8	Outage	-	-	1-Oct-00	3-Mar-21	-	7,458.00	-

*Irradiation days correspond to reactor operation days and not calendar days between cycles

5.1.3 CALCULATIONS AND RESULTS

The first step was to determine the neutron distribution across the reflector cage. Based on that distribution, the highest flux region values for the aluminum and stainless-steel cases were determined. The neutron flux values were calculated using the tally type 4 results extracted from both cases' MCNP (X-5 Monte Carlo Team, 2005) output files. The type F4 tally in MCNP (X-5 Monte Carlo Team, 2005) reports the average flux in a particular region of interest (cell). The number computed then is normalized to the desired power (100 MW) using Eqs. (1) and (2) shown below:

$$S\left[\frac{neutrons}{sec}\right] = \frac{P[MW]\bar{\upsilon}\left[\frac{neutrons}{fission}\right]}{1.6022 \times 10^{-19}\left[\frac{MJ}{MeV}\right]Q_T\left[\frac{MeV}{fission}\right]}, \text{ where} \quad (1)$$

S = number of neutrons being produced per second from fissioning,
P = total reactor power,
$\bar{\upsilon}$ = average number of neutrons produced per fission,
Q_T = average energy released per fission, and

$$\phi_{neutron\ Flux}\left(\frac{neutrons}{cm^2 - sec}\right) = S\left[\frac{neutrons}{sec}\right] * \left(F4\ tally\ \frac{neutrons}{cm^2 - neutrons}\right). \quad (2)$$

The fluxes were extracted from the simulation results and normalized to 100 MW reactor power using Eqs. (1) and (2). The results of those calculations are presented in Table 6.

Table 6. Reflector container regions flux results

Volumetric region	Cell number	Volume (cm^3)	Neutron flux aluminum (neutron/cm^{2-s})	Neutron flux stainless steel (neutron/cm^{2-s})
1	41200	6987.19	2.65E+08	1.98E+08
2	41201	6987.09	4.33E+08	1.57E+08
3	41202	6987.34	4.53E+08	3.30E+08
4	41203	6986.18	3.79E+08	1.91E+08
5	41210	6986.97	9.92E+10	5.09E+10
6	41211	6987.01	9.46E+10	4.92E+10
7	41212	6988.19	9.60E+10	5.05E+10
8	41213	6988.52	9.69E+10	5.05E+10
9	41220	3493.76	1.52E+13	5.82E+12
10	41221	3493.36	1.27E+13	4.97E+12
11	41222	3319.43	1.57E+13	6.09E+12
12	41223	3494.51	1.38E+13	5.31E+12
13	41230	3149.3	9.01E+13	4.01E+13
14	41231	2981.47	6.93E+13	3.12E+13
15	41232	2449	1.11E+14	5.00E+13
16	41233	3213.06	7.72E+13	3.42E+13
17	41240	3149.39	8.94E+13	3.98E+13
18	41241	2725.42	7.28E+13	3.27E+13
19	41242	2706.15	1.06E+14	4.73E+13
20	41243	3212.1	7.67E+13	3.40E+13
21	41250	3493.2	1.48E+13	5.66E+12
22	41251	3408.45	1.20E+13	4.73E+12
23	41252	3406.64	1.63E+13	6.18E+12
24	41253	3493.54	1.35E+13	5.20E+12
25	41260	6987.05	8.99E+10	4.83E+10
26	41261	6986.64	8.86E+10	4.64E+10
27	41262	6987.49	9.35E+10	4.80E+10
28	41263	6986.55	8.87E+10	4.65E+10
29	41270	6987.01	6.30E+08	2.54E+08
30	41271	6988.37	3.44E+08	1.89E+08
31	41272	6986.78	2.90E+08	2.76E+08
32	41273	6987.84	2.83E+08	1.42E+08
33	8215	1098.19	3.65E+13	1.44E+13
34	8235	1098.19	2.04E+13	8.09E+12

Table 6 also contains the volumes for each region. Based on the results shown in Table 6, the highest neutron flux region for both cases can be found in cell 41232 (axial and radial locations are shown in orange in Figure 6 a and b). It is important to point out that as the stainless-steel fraction increases so are the self-shielding effects in the beryllium reflector container. This could cause an underestimation of the flux for the stainless-steel cases.

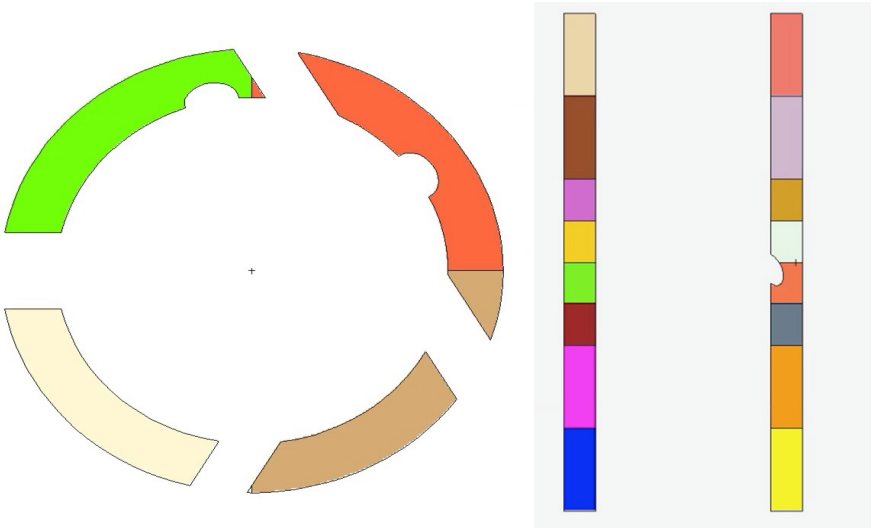

Figure 6. Reflector container regions: (a) radial (left) and (b) horizontal (right).

Using the maximum flux region along with the 44-discretized flux group and mass density of each material, the total curie and isotopic contents per cm^3 were calculated. As shown in the Figure 5 flowchart, the energy discretized group flux was used as an input for the COUPLE program. Results from the COUPLE program were included with the maximum region total flux and the mass density of both materials as input for ORIGEN-S (Hermann, O.W., 1984), which was then used to compute the total curie and isotopic inventory per cm^3 for the stainless steel and aluminum cases.

Table 7. (100%) Irradiated Aluminum Isotopic Distribution

Aluminum	**Curie content per volume on 3-Mar-21**
Isotopes	Ci/cm3
h-3	8.88E-06
al-26	9.20E-09
si-32	2.35E-11
p-32	2.35E-11
fe-55	1.44E-04
fe-60	1.66E-10
co-60	1.10E-04
co-60m	1.66E-10
ni-63	2.30E-06
zn-65	2.08E-11
Total	2.65E-04

Table 7 and Table 8 contain the total activity per cm^3, as well as the isotopic breakdown, for the aluminum and stainless-steel cases, respectively.

Table 8. (100%) Stainless steel isotopic distribution.

Stainless Steel 304	Curie content per volume on 3-Mar-21
Isotopes	Ci/cm^3
h-3	3.46E-06
c-14	1.22E-08
fe-55	5.32E-01
co-60	1.12E-02
ni-59	1.66E-03
ni-63	4.61E-01
Total	1.0056

Table 9. Beryllium reflector SolidWorks calculated volume (0).

Beryllium reflector parts	Calculated volume (in^3)	Calculated volume (cm^3)
Cage	3,794.51	62,181.01
Pedestal	5,793.22	9,4934.08
Total volume	9,587.73	157,115.09

Finally, the total curie and isotopic distribution for the 100% aluminum and stainless-steel cases—along with the total estimated beryllium reflector volume shown in Table 9—were used to compute the total activity (Table 10) and isotopic breakdown (Table 11) for a range of material volumetric fractions.

Table 10. Total Activity Results.

Vol % Aluminum	Vol % SS	Aluminum Volume (cm^3)	Stainless Steel Volume (cm^3)	Activity (Ci) Al	Activity (Ci) Stainless Steel	Total Activity (Ci)
99.20%	0.80%	155,858.17	1,256.92	41.34	1,263.92	1,305.26
99.30%	0.70%	156,015.28	1,099.81	41.38	1,105.93	1,147.31
99.40%	0.60%	156,172.40	942.69	41.42	947.94	989.36
99.50%	0.50%	156,329.51	785.58	41.46	789.95	831.41
99.60%	0.40%	156,486.63	628.46	41.51	631.96	673.47
99.70%	0.30%	156,643.75	471.35	41.55	473.97	515.52
99.80%	0.20%	156,800.86	314.23	41.59	315.98	357.57
99.90%	0.10%	156,957.98	157.12	41.63	157.99	199.62
99.98%	0.02%	157,083.67	31.42	41.66	31.60	73.26
100.00%	0.00%	157,115.09	0.00	41.67	0.00	41.67

Table 11. Isotopic Curie Content for different volumetric fractions.

	Al %	Al %	Al %	Al %	Al %	Al %	Al %	Al %	Al %	Al %
Isotopes	**99.20%**	**99.30%**	**99.40%**	**99.50%**	**99.60%**	**99.70%**	**99.80%**	**99.90%**	**99.98%**	**100.00%**
h-3	1.39E+00	1.39E+00	1.39E+00	1.39E+00	1.39E+00	1.39E+00	1.39E+00	1.39E+00	1.40E+00	1.40E+00
c-14	1.53E-05	1.34E-05	1.15E-05	9.59E-06	7.67E-06	5.75E-06	3.84E-06	1.92E-06	3.84E-07	0.00E+00
fe-55	6.91E+02	6.08E+02	5.24E+02	4.41E+02	3.57E+02	2.73E+02	1.90E+02	1.06E+02	3.94E+01	2.27E+01
co-60	3.12E+01	2.94E+01	2.77E+01	2.59E+01	2.42E+01	2.25E+01	2.07E+01	1.90E+01	1.76E+01	1.72E+01
ni-59	2.08E+00	1.82E+00	1.56E+00	1.30E+00	1.04E+00	7.80E-01	5.20E-01	2.60E-01	5.20E-02	0.00E+00
ni-63	5.79E+02	5.07E+02	4.35E+02	3.62E+02	2.90E+02	2.18E+02	1.45E+02	7.27E+01	1.48E+01	3.62E-01
al-26	1.43E-03	1.43E-03	1.44E-03	1.44E-03	1.44E-03	1.44E-03	1.44E-03	1.44E-03	1.44E-03	1.45E-03
si-32	3.66E-06	3.66E-06	3.66E-06	3.67E-06	3.67E-06	3.68E-06	3.68E-06	3.68E-06	3.69E-06	3.69E-06
p-32	3.66E-06	3.66E-06	3.67E-06	3.67E-06	3.67E-06	3.68E-06	3.68E-06	3.68E-06	3.69E-06	3.69E-06
fe-60	2.58E-05	2.58E-05	2.59E-05	2.59E-05	2.59E-05	2.59E-05	2.60E-05	2.60E-05	2.60E-05	2.60E-05
co-60m	2.58E-05	2.58E-05	2.59E-05	2.59E-05	2.59E-05	2.59E-05	2.60E-05	2.60E-05	2.60E-05	2.60E-05
zn-65	3.24E-06	3.25E-06	3.25E-06	3.25E-06	3.25E-06	3.26E-06	3.26E-06	3.26E-06	3.27E-06	3.27E-06
Total	1305.26	1147.31	989.36	831.41	673.46	515.52	357.57	199.62	73.26	41.67

6. COMPARISON OF MCNP-ORIGEN ANALYSIS AND MICROSHIELD RESULTS

Both computational methodologies used to estimate the total activity are sensitive to the volumetric fraction assumption between aluminum and stainless steel. The methodology used in Section 4 is particularly sensitive compared to the dose-to-curie methodology, as can be seen in Figure 7.

Figure 7 shows the predictions' results for both methodologies based on different volumetric material fractions. Both curves predict activity, but their methodologies use different initial information to perform the analysis. The MicroShield analysis uses experimental information based on the state of the reflector container at the time the measurements were taken (present), whereas the activation methodology uses historical information (past) as initial inputs. Figure 7 also shows that the activation analysis is the bounding case and while self-shielding effects were overestimated for the stainless-steel cases the conservatism used during the analysis out weighted those effects.

For both methods, the volumetric ratio is also an input, but neither methodology by itself could determine which is the current volumetric fraction of aluminum / stainless steel in the reflector container. For the MicroShield analysis, the true volumetric fraction is embedded within the exposure rate information used as an input parameter. Therefore, the true state of the system at the time of the measurements will only occur with the correct volumetric fraction. On the other hand, the activation analysis predicts different activities for a range of volume fractions. Consequently, only the true aluminum stainless-steel volumetric fraction will yield the activity prediction corresponding to the current state of the reflector container.

This means that both curves should only be near to or converging in the region of the plot in which the aluminum fractions are similar to or equal to each other. Based on that theory, the regions between 99.90% and 100% aluminum shown in Figure 7 are the area of the curves that contain the actual aluminum/stainless volume fraction of the beryllium container.

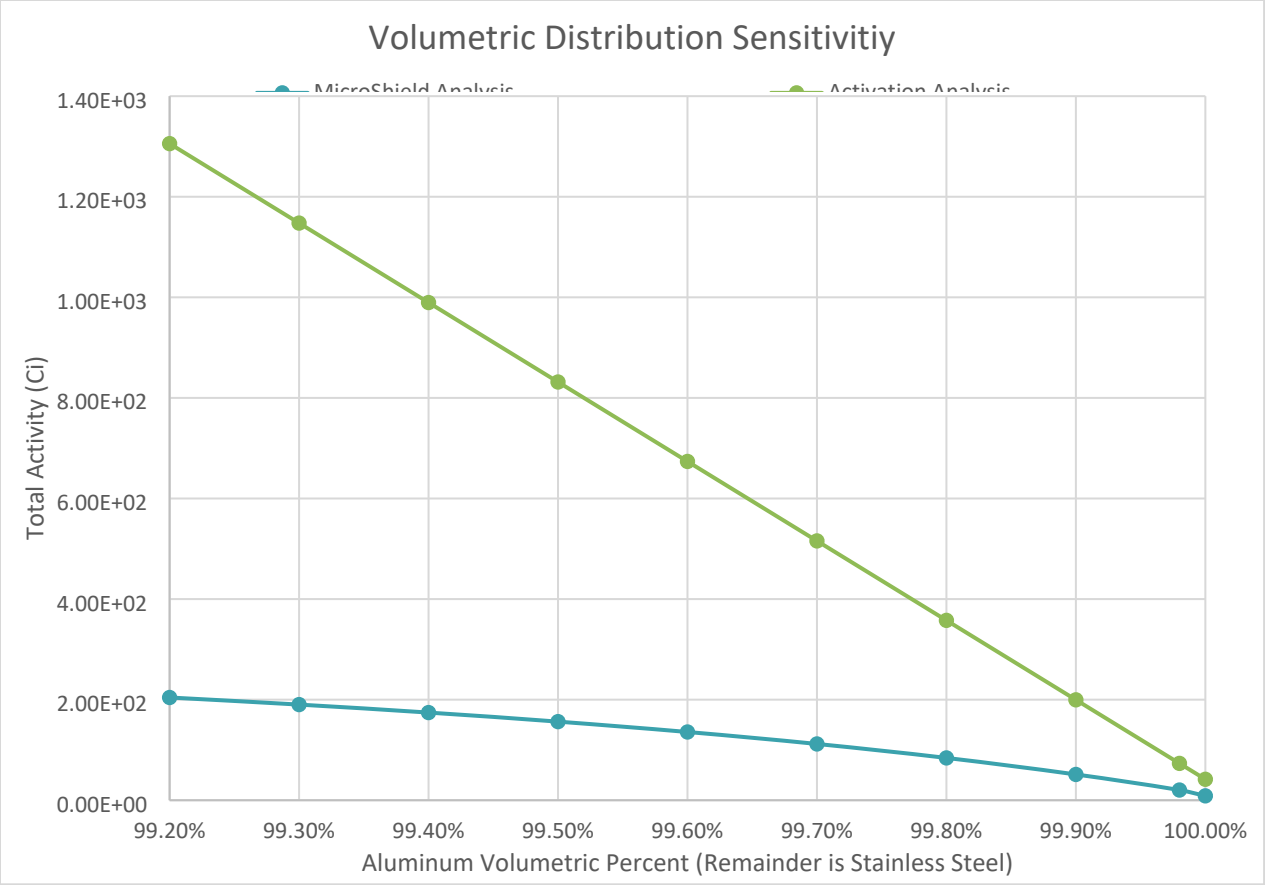

Figure 7. Volumetric distribution sensitivity for both methodologies.

7. CONCLUSIONS AND RECOMMENDATIONS

An approach to determine a conservative scenario of the total isotopic activity content, as well as current volumetric fractions, was developed and applied. The methodology presented in this report was based on using different sources of experimental and simulation methods to better understand the state of the system. By using and comparing the different sources of information, it was concluded the data point of 205.54 Ci corresponding to the aluminum volumetric fraction of 99.9% is a bounding activity estimate, with the actual activity being closer to 51.3 Ci as determined with the exposure-to-curie calculation. A conservative isotopic inventory corresponding to that volumetric fraction (Table 11) was also determined. In addition, a conservatively higher ^{60}Co activity than the experiment-based methodology was also calculated. In summary, the conservative total activity of 205.54 Ci and its isotopic inventory corresponding to the aluminum volumetric fraction of 99.9% can be used as the baseline for the beryllium reflector container disposal activities.

8. WORKS CITED

1. Ilas, G, Chandler, D., et. al., (2015). *Modeling and Simulations for the High Flux Isotope Reactor Cycle 400*. Oak Ridge National Laboratory, Oak Ridge, TN (ORNL/TM-2015/36).
2. Hermann, O. (1984). *COUPLE: SCALE System Module to process Problem-Dependent Cross Sections and Neutron Spectral Data for ORIGEN-S Analyses.* Oak Ridge National Laboratory, Oak Ridge, TN (NUREG/CR--0200-Vol. 2).
3. Hermann, O.W., & Westfall, R.M. (1984). *ORIGEN-S: SCALE system module to calculate fuel depletion, actinide transmutation, fission product buildup and decay, and associated radiation source terms.* Oak Ridge National Laboratory, Oak Ridge, TN (NUREG/CR--0200-Vol2).
4. Grove Software (2006), *MicroShield 7.01. User's Manual*.
5. X-5 Monte Carlo Team (2005), *MCNP—A General Monte Carlo N-Particle Transport Code, Version 5*. Los Alamos National Laboratory, Los Alamos.

APPENDIX A. EMAIL CONTAINING SOLIDWORKS MODEL INFORMATION FROM GEOFFREY G. DEICHERT

Cage Analysis Next Steps

Deichert, Geoffrey G. <deichertgg@ornl.gov>
Thu 1/28/2021 1:17 PM

To: Navarro, Jorge <navarroj@ornl.gov>
Cc: Pudelek, Randal E. <pudeleke@ornl.gov>; Kwon, Young Soo <kwonys@ornl.gov>; Wools, Russ <woolsrl@ornl.gov>; Sowers, Tina <sowerstm@ornl.gov>; Grooms, Matthew A. <groomsma@ornl.gov>; Blanchard, David G. <blanchardg@ornl.gov>

5 attachments (9 MB)
CageAnalysisJN_1_20_21.pptx; Aluminum and SS Character.xlsx; RE: Heli Coil SS; pins bolts keys helicoils.pdf; Cage and Can Rad Survey 17June2020.pdf;

Jorge,
For Next Step Items 1 and 2 in your powerpoint presentation:

Solidworks model realistic volume of cage = 3794.51 cu in; pedestal = 5793.22 cu in; and can = 253.02 cu in.

Calculated fractional volume from Randy's spreadsheet: 99.7% Aluminum and 0.26% Stainless. There may be residual stainless particles left on the aluminum from heli coils, bolts, pins, O-ring, washers, hex screws and nuts or other reactor parts in contact with the cage. However, I can not explain the higher dose rates at the center of the cage with respect to the stainless steel part locations (cage top and cage bottom) although I suspect activation from the beam lines or EFs play a role. Another explanation is a cumulative effect from both top and bottom locations to the center.

The location of the heli coils (23 remain of 24) are in the top of the cage and are 300 series Stainless Steel. The keys (2 of 2) remaining are made of 6061 Aluminum. The bolts (3 of 8) and pins (2 of 8) that remain are 303 and 302 Stainless Steel, respectively.

Thanks,
Geoff

Geoffrey G. Deichert
Systems Engineer and Shift Technical Advisor
Research Reactors Division
High Flux Isotope Reactor (HFIR)

Oak Ridge National Laboratory
1 Bethel Valley Road
Bldg 7964J, Rm 012
PO Box 2008, MS6394
Oak Ridge, TN 37831-6394

(865)241-3946
deichertgg@ornl.gov

Notes:

*The stainless-steel fraction calculation shown in this email was performed prior to the stainless-steel removal operation
* The higher dose at the center of the cage was taken into consideration while developing the conservative methodology approach. The activation analysis found that the highest flux area was at the EF section and it used that upper bound flux as a basis for the calculations.

APPENDIX B. MICROSHIELD OUTPUT

MicroShield 8.03
ORNL (8.03-0000)

Date	By	Checked

Filename	Run Date	Run Time	Duration
CAGE w ped.msd	April 26, 2021	12:11:01 PM	00:00:00

Project Info

Case Title	CAGE DTC
Description	2-meter exposure rate from 1 Ci Co-60
Geometry	12 - Annular Cylinder - External Dose Point

Source Dimensions

Height	153.353 cm (5 ft 0.4 in)
Inner Cyl Radius	54.293 cm (1 ft 9.4 in)
Inner Cyl Thickness	0.0 cm (0 in)
Outer Cyl Thickness	0.0 cm (0 in)
Source	12.065 cm (4.8 in)

Dose Points

A	X	Y	Z
#1	260.325 cm (8 ft 6.5 in)	109.538 cm (3 ft 7.1 in)	0.0 cm (0 in)

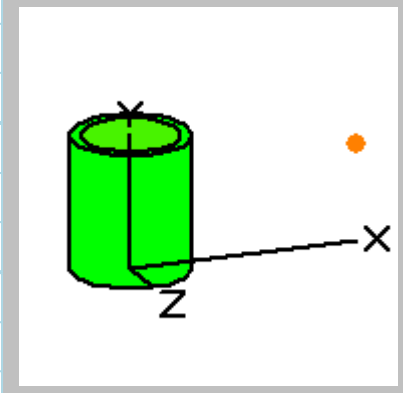

Shields

Shield N	Dimension	Material	Density
Cyl. Radius	54.293 cm	Air	0.00122
Source	7.01e+05 cm³	Aluminum	1.15
Transition		Air	0.00122
Air Gap		Air	0.00122

Source Input: Grouping Method - Actual Photon Energies

Nuclide	Ci	Bq	µCi/cm³	Bq/cm³
Co-60	1.0000e+000	3.7000e+010	1.4260e+000	5.2760e+004

Buildup: The material reference is Source
Integration Parameters

Radial	10
Circumferential	20

Y Direction (axial)					20
Results					
Energy (MeV)	**Activity (Photons/sec)**	**Fluence Rate MeV/cm²/sec No Buildup**	**Fluence Rate MeV/cm²/sec With Buildup**	**Exposure Rate mR/hr No Buildup**	**Exposure Rate mR/hr With Buildup**
0.6938	6.035e+06	1.657e+00	3.139e+00	3.199e-03	6.060e-03
1.1732	3.700e+10	2.056e+04	3.359e+04	3.674e+01	6.003e+01
1.3325	3.700e+10	2.438e+04	3.853e+04	4.229e+01	6.685e+01
Totals	**7.401e+10**	**4.494e+04**	**7.213e+04**	**7.903e+01**	**1.269e+02**